

Laminar–Turbulent Transition Control Using Passivity Analysis of the Orr–Sommerfeld Equation

Christopher J. Damaren*

University of Toronto, Toronto, Ontario M3H 5T6, Canada

DOI: 10.2514/1.G001763

The control problem for linearized two-dimensional wall-bounded parallel shear flows is considered as a means of preventing the laminar-to-turbulent transition. The linearized Navier–Stokes equations are reduced to the Orr–Sommerfeld equation with wall-normal velocity actuation entering through the boundary conditions on the wall. An analysis of the work-energy balance is used to identify appropriate sensor outputs that could lead to a passive closed-loop system using simple feedback laws. These sensor outputs correspond to the second spatial derivative (normal direction) of the streamwise velocity at the wall, and it is demonstrated that they can be realized by pressure measurements made at appropriate locations along the wall. Spatial discretization of the Orr–Sommerfeld equation in the wall-normal direction is accomplished using Hermite cubic finite elements, and the resulting spectrum is shown to agree with literature values for both plane Poiseuille flow and the Blasius boundary layer. Both cases are shown to be stabilized by simple constant-gain output feedback using the special choice of sensor measurement. In each case, this holds for a single gain and a wide range of Reynolds numbers and wave numbers. However, the closed-loop system produced in the Poiseuille case is shown to be passive (i.e., it has a positive-real transfer function), whereas in the Blasius case, it is nonminimum-phase and hence is not passive.

I. Introduction

IT IS well known that the skin friction drag produced by wall-bounded shear flows greatly depends on whether the flow is laminar or turbulent, with the former producing less drag. One way of studying the transition between the two types of flow is by examining the instability of small perturbations produced about a nominal laminar flow. This can be performed by determining the eigenvalues of the linearized model governing the perturbations [1]. In two dimensions with a nominal parallel flow, this approach leads to consideration of the Orr–Sommerfeld equation. In this light, a possible approach to preventing or spatially delaying transition is to prevent the instability from occurring via the introduction of appropriate sensors and actuators as well as the use of active feedback control [2]. From a control systems perspective, the problem is one of feedback stabilization by output feedback.

The Orr–Sommerfeld equation results from the two-dimensional linearized Navier–Stokes equations, where the base flow is a parallel shear flow. It is developed from the assumption that perturbations in the streamwise direction are oscillatory in the horizontal spatial coordinate, and historically it has been studied by also assuming time-harmonic solutions. This leads to an eigenproblem that is usually identified as the Orr–Sommerfeld equation. The study of this eigenproblem occupied the better part of flow transition studies in the last century and is detailed in [1]. In particular, much work was centered on determining the critical values of the Reynolds number and wave number that led to instability and transition.

When researchers began to study active feedback control as a means of preventing the transition by stabilization, it seemed natural to use the linearized Navier–Stokes equation and its creations: the Orr–Sommerfeld equation and its cousin, the Squire system of equations. The latter occurs when one considers three-dimensional perturbations and describes the spanwise behavior; it is coupled to the

Orr–Sommerfeld equation. The history and use of both equations in developing linear state-space models of a flow control problems is described in [2].

The two most studied flows in the context of active control design using the Orr–Sommerfeld equation are plane Poiseuille flow [3,4] and the Blasius boundary layer [5,6]. This paper will consider both flows. Both are parallel shear flows described in [1]. The Poiseuille flow corresponds to the fully developed flow in a channel between two parallel infinite plates (this will be described in more detail in Sec. III.B). The Blasius boundary layer is the two-dimensional laminar flow over a semi-infinite flat plate (this will be described in more detail in Sec. III.C). Although not strictly a parallel flow, it will be treated as such in this work.

It may seem odd that we propose to use two-dimensional modeling and linear stability analysis as the basis for a controller design, when it is now widely recognized that transition to turbulence is a nonlinear, three-dimensional phenomenon [7]. In fact, it is generally recognized that transition typically occurs before the critical Reynolds number predicted by linear theory and arises from the large transient energy growth due to the nonnormal nature of the equations involved. This leads to nonlinear behavior, which leads to turbulence. Despite this scenario, many authors have argued that, for control system design, linear models “might well be good enough” [8]. The reasoning is that linear control systems can deal with the initial stage of the process (linear amplification of disturbances), thus preventing the subsequent nonlinear transition behavior. The justification of a two-dimensional approach that ignores the Squire system is Squire’s theorem, which states that the critical Reynolds number in the two-dimensional analysis is always less than that in the corresponding three-dimensional analysis [1]. In [3], linear feedback controllers developed using a two-dimensional model of Poiseuille flow were shown to attenuate finite two-dimensional perturbations.

Many of the important characteristics of a control problem are governed by the type and location of the sensors and actuators. In a linear time-invariant (LTI) control problem, the location of the zeros of the corresponding transfer function (matrix) are affected by these things. In particular, zeros located in the right half of the complex plane lead to the nonminimum-phase property, which leads to instability when high-gain output feedback is used. Stable systems with a stable inverse are termed minimum-phase and are easier to control. In the LTI case, the corresponding transfer function has no poles or zeros in the open right half-plane. Sensor and actuator location has been considered by [3] in the Poiseuille case and [6] in the Blasius case.

Received 7 October 2015; revision received 1 February 2016; accepted for publication 2 February 2016; published online 28 March 2016. Copyright © 2016 by Christopher J. Damaren. Published by the American Institute of Aeronautics and Astronautics, Inc., with permission. Copies of this paper may be made for personal and internal use, on condition that the copier pay the per-copy fee to the Copyright Clearance Center (CCC). All requests for copying and permission to reprint should be submitted to CCC at www.copyright.com; employ the ISSN 0731-5090 (print) or 1533-3884 (online) to initiate your request.

*Professor, Institute for Aerospace Studies, 4925 Dufferin Street. Associate Fellow AIAA.

An important class of systems enjoy the property of passivity and are termed passive [9]. Such systems only store or dissipate energy, and the study of this property originated in the field of passive electrical circuits [10]. A stronger property than passivity is strict passivity, which corresponds to systems that only consume (dissipate) energy. The celebrated passivity theorem [9] states that the negative feedback interconnection of a passive system and a strictly passive system is L_2 -stable, where L_2 is the space of temporally square-integrable functions; that is, L_2 inputs produce L_2 outputs (finite energy inputs produce finite energy outputs). Hence, passive systems can be stabilized by a simple constant-gain negative output feedback (the simplest strictly passive system).

In the control of mechanical systems within the realm of solid mechanics, linear elastic structures with collocated force inputs and velocity outputs (or collocated torque inputs and angular velocity outputs) are passive [11]. They can be robustly stabilized by strictly passive negative feedback because the passivity property is present regardless of the details of the mass distribution, vibration frequencies, mode shapes, and number of modes maintained in the spatial discretization. Hence, so-called spillover instabilities, produced by a lower-order controller applied to a structure containing vibration modes other than those used to design the controller, are avoided.

Given the utility of the passivity property, we examine the possibility of obtaining it in the context of the Orr–Sommerfeld equation, where the actuation is implemented by varying the wall-normal velocity. A fundamental question is what are the corresponding sensor outputs that could potentially lead to a passive system? We answer this question by examining the work-energy balance of the Orr–Sommerfeld equation. The relevant outputs are shown to be the second spatial derivative (normal direction) of the streamwise velocity perturbation at the wall, and it is demonstrated that they can be realized by pressure measurements made at appropriate locations along the wall. Although passivity cannot be achieved for the open-loop system, it is numerically demonstrated that an appropriate closed-loop system enjoys this property in the Poiseuille case but not in the Blasius case.

For our numerical examples, spatial discretization of the Orr–Sommerfeld equation in the wall-normal direction is accomplished using Hermite cubic finite elements, which were originally used for Poiseuille flows in [12]. Our application to controlled flows and the Blasius boundary layer is novel. The resulting eigenvalue spectra are shown to agree with literature values for both plane Poiseuille flow and the Blasius boundary layer. From the control standpoint, these two cases are shown to have some fundamental differences. Both are shown to be stabilized by simple constant-gain output feedback using the special choice of sensor measurements. However, the closed-loop system produced in the Poiseuille case is shown to be passive (i.e., it has a positive-real transfer function), whereas in the Blasius case, it is nonminimum-phase and hence is not passive. This is our main contribution. Passivity ideas have been employed in [13] in the stabilization of a Poiseuille flow where dynamic linear controller designs were employed to render the closed-loop system to be passive.

The paper is organized as follows. Section II defines and illustrates the key notions involving passivity in the context of controlling flexible structures, a well known application. Section III develops the Orr–Sommerfeld equation, and by using energy as a storage function, a key set of inputs and outputs are defined for use in a passivity-based control strategy. They are then interpreted as physical quantities, namely wall-normal velocity inputs and specially chosen pressure measurements. Section IV presents the spatial discretization of the Orr–Sommerfeld equation based on the finite element method. The closed-loop state-space equations for Poiseuille and Blasius flows are developed in Sec. V for the simplest feedback strategy, the use of a single gain. The eigenvalues are numerically calculated as a function of Reynolds number, wave number, and feedback gain. Stability diagrams and root locus plots are presented for both flow types. Time-domain simulations are presented in Sec. VI, and Sec. VII presents some concluding remarks.

II. Passivity-Based Control

A. Input-Output Stability Theory

Consider a vector function of time $z(t)$. We have that $z \in L_2$ if the L_2 -norm satisfies $\|z\|_2 = \sqrt{\int_0^\infty z^T(t)z(t) dt} < \infty$; we use the symbol $()^T$ to denote the matrix transpose and $()^H$ to denote the complex-conjugate transpose. In addition, $z \in L_{2e}$ (the extended L_2 -space) if $\|z\|_{2T} = \sqrt{\int_0^T z^T(t)z(t) dt} < \infty, 0 \leq T < \infty$. Note that $L_2 \subset L_{2e}$. Consider a system $z(t) = (\mathcal{G}\nu)(t)$ where the operator $\mathcal{G}: L_{2e} \rightarrow L_{2e}$ (possibly nonlinear and time-varying) maps the input $\nu \in L_{2e}$ into the output $z \in L_{2e}$ (note that the symbol ν will not be used in this paper to refer to a fluid’s kinematic viscosity). For a square system (the number of inputs is equal to the number of outputs), the operator \mathcal{G} is defined to be strictly passive if $\int_0^T z^T(t)\nu(t) dt \geq \beta + \epsilon \int_0^T \nu^T(t)\nu(t) dt, 0 \leq T < \infty$ for some $\epsilon > 0$ and real constant β . If this property is satisfied with $\epsilon = 0$, then the system is passive. The system is L_2 -stable if $\nu \in L_2$ implies that $z = \mathcal{G}\nu \in L_2$.

Linear time-invariant (LTI) systems can be described using transfer functions: $z(s) = G(s)\nu(s)$ where $z(s)$ denotes the Laplace transform of $z(t)$ (a common abuse of notation) and $G(s)$ is the system transfer (function) matrix. The quantity s denotes the complex-valued Laplace transform variable and $i = \sqrt{-1}$. Note that $G(s) = C(sI - A)^{-1}B + D$ for LTI systems described by the standard state-space model $\dot{x}(t) = Ax(t) + B\nu(t), z(t) = Cx(t) + D\nu(t)$. Here, I is the identity matrix of appropriate dimension, and (\cdot) denotes the time derivative. If the system is minimal (i.e., it is controllable and observable), then L_2 -stability corresponds to the matrix A having eigenvalues with negative-real parts.

Passive LTI systems of this form correspond to the case where $G(s)$ is a positive-real (PR) transfer function. When $G(s)$ is a proper real rational matrix function of s , it is positive-real if no element of $G(s)$ has a pole in $\Re\{s\} > 0; He[G(i\omega)] = (1/2)[G(i\omega) + G^H(i\omega)] \geq \mathbf{0}$ for all real ω with $i\omega$ not a pole of $G(s)$ ($He(\cdot)$ denotes the Hermitian part of a square matrix); and if $i\omega_0$ is a pole of any element of $G(s)$, it is at most a simple pole and the residue matrix $\lim_{s \rightarrow i\omega_0} (s - i\omega_0)G(s)$ is nonnegative-definite Hermitian. A stronger property than positive-real is strictly positive-real (SPR). A proper real rational matrix function of s is SPR if no element of $G(s)$ has a pole in $\Re\{s\} \geq 0; He[G(i\omega)] > \mathbf{0}$ for all real $\omega \in (-\infty, \infty)$; and $\lim_{\omega \rightarrow \infty} \omega^2 He[G(i\omega)] > \mathbf{0}$.

The importance of passivity for feedback design lies in the celebrated passivity theorem [9], which addresses the feedback system shown in Fig. 1. It may be described by $z = \mathcal{G}(d - \mathcal{H}z)$ for operators $\mathcal{G}: L_{2e} \rightarrow L_{2e}$ and $\mathcal{H}: L_{2e} \rightarrow L_{2e}$. The passivity theorem states that, if \mathcal{G} is passive and \mathcal{H} is strictly passive, then $d \in L_2$ implies that $z \in L_2$. It can be shown that this stability property holds if \mathcal{G} corresponds to an LTI system with an SPR transfer matrix, and \mathcal{H} corresponds to an LTI system with a PR transfer matrix [14].

Another important problem is the selection of the feedback operator \mathcal{H} so that the closed-loop system (i.e., the mapping from d to z) is passive. This has important ramifications for disturbance rejection and the robustness of the stabilization with respect to passive perturbations Δ modeled as negative feedback around \mathcal{G} . For example, if in Fig. 2, Δ is a passive system and the negative feedback interconnection of \mathcal{G} and \mathcal{H} is strictly passive, then $d \in L_2$ implies that $z \in L_2$. This has ramifications for our problem because, in [13], it is noted that, in some cases, the nonlinearities in the Navier–Stokes

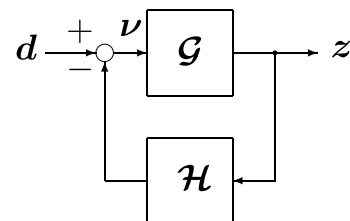


Fig. 1 Feedback system.

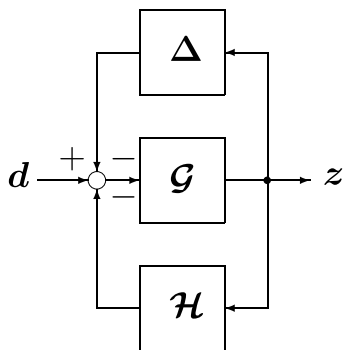


Fig. 2 Feedback system with passive feedback perturbation.

equations can be shown to be a passive negative feedback around a nominal model based on the linearized Navier–Stokes equations.

B. Example of Passivity Analysis in the Control of Flexible Structures

Historically, a key application of passivity in the control of mechanical systems has been the control of flexible structures using collocated actuators and sensors. In this subsection, we summarize the passivity analysis in this case because it may be familiar to many readers and is key motivation for our approach to the fluid-control problem in the next section. This subsection will highlight the relationship of a positive-real transfer function to a passive system, the use of energy as a storage function for establishing passivity, and the role of collocated (dual) actuators and sensors in producing a passive system.

Consider a constrained (no rigid-body motion permitted) linear elastic flexible structure with deformation field $\mathbf{w}(\mathbf{r}, t) = [w_1 \ w_2 \ w_3]^T$, where the spatial coordinates are given by $\mathbf{r} = [r_1 \ r_2 \ r_3]^T$. It occupies an undeformed volume V . It is assumed that a force actuator acts at location \mathbf{r}_a in the direction \mathbf{n}_a with a force given by $\nu(t)$. The partial differential equation (PDE) describing the motion [15] is

$$\mathcal{M}\ddot{\mathbf{w}}(\mathbf{r}, t) + \mathcal{D}\dot{\mathbf{w}}(\mathbf{r}, t) + \mathcal{K}\mathbf{w}(\mathbf{r}, t) = \mathbf{n}_a\delta(\mathbf{r} - \mathbf{r}_a)\nu(t) \quad (1)$$

Here, \mathcal{M} is the mass operator, \mathcal{D} is the damping operator, and \mathcal{K} is the stiffness operator, all of which are assumed to be self-adjoint, positive-definite, and may contain spatial partial derivatives. In addition, $\delta(\mathbf{r})$ denotes the Dirac delta function. The output measurement is taken to be a velocity measurement at location \mathbf{r}_s in the direction \mathbf{n}_s :

$$z(t) = \mathbf{n}_s^T \dot{\mathbf{w}}(\mathbf{r}_s, t) \quad (2)$$

The undamped eigenvalue problem corresponding to the undamped, unforced version of Eq. (1) is

$$-\omega_\alpha^2 \mathcal{M}\psi_\alpha + \mathcal{K}\psi_\alpha = \mathbf{0}, \quad \alpha = 1, 2, 3, \dots \quad (3)$$

where $\omega_\alpha > 0$ are the undamped natural frequencies, and ψ_α are the undamped eigenfunctions. The orthogonality relations are taken to be

$$\int_V \psi_\alpha^T \mathcal{M} \psi_\beta \, dV = \delta_{\alpha\beta}, \quad (4)$$

$$\int_V \psi_\alpha^T \mathcal{K} \psi_\beta \, dV = \omega_\alpha^2 \delta_{\alpha\beta} \quad (5)$$

$$\int_V \psi_\alpha^T \mathcal{D} \psi_\beta \, dV = 2\zeta_\alpha \omega_\alpha \delta_{\alpha\beta}, \quad (6)$$

where $\zeta_\alpha > 0$ are the modal damping ratios, and $\delta_{\alpha\beta}$ is the Kronecker delta. Although the undamped eigenfunctions are not guaranteed to possess orthogonality with respect to the damping operator, it is

assumed to be the case here for simplicity of exposition. This would happen, for example, when \mathcal{D} is a linear combination of \mathcal{M} and \mathcal{K} .

We adopt the modal expansion

$$\mathbf{w}(\mathbf{r}, t) = \sum_{\alpha=1}^{\infty} \psi_\alpha(\mathbf{r}) \eta_\alpha(t) \quad (7)$$

where $\eta_\alpha(t)$ are the modal coordinates. Substituting this into the sensor Eq. (2) leads to

$$z(t) = \sum_{\alpha=1}^{\infty} \mathbf{n}_s^T \psi_\alpha(\mathbf{r}_s) \dot{\eta}_\alpha(t) \quad (8)$$

$$= \sum_{\alpha=1}^{\infty} \psi_{s,\alpha} \dot{\eta}_\alpha(t), \quad \psi_{s,\alpha} = \mathbf{n}_s^T \psi_\alpha(\mathbf{r}_s) \quad (9)$$

Substituting the modal expansion [Eq. (7)] into the PDE in Eq. (1), premultiplying by ψ_α^T and integrating over V while using the orthogonality relations, leads to the modal equations of motion:

$$\ddot{\eta}_\alpha(t) + 2\zeta_\alpha \omega_\alpha \dot{\eta}_\alpha(t) + \omega_\alpha^2 \eta_\alpha(t) = \psi_{a,\alpha} \nu(t), \quad \alpha = 1, 2, 3, \dots \quad (10)$$

where $\psi_{a,\alpha} = \mathbf{n}_a^T \psi_\alpha(\mathbf{r}_a)$.

Taking Laplace transforms of Eqs. (9) and (10) gives

$$z(s) = \sum_{\alpha=1}^{\infty} s \psi_{s,\alpha} \eta_\alpha(s)$$

$$\eta_\alpha(s) = \frac{\psi_{a,\alpha}}{s^2 + 2\zeta_\alpha \omega_\alpha s + \omega_\alpha^2} \nu(s), \quad \alpha = 1, 2, 3, \dots$$

Combining these yields

$$z(s) = \left[\sum_{\alpha=1}^{\infty} \frac{s C_\alpha}{s^2 + 2\zeta_\alpha \omega_\alpha s + \omega_\alpha^2} \right] \nu(s), \quad C_\alpha = \psi_{s,\alpha} \psi_{a,\alpha} \quad (11)$$

The bracketed expression is the relevant transfer function relating the input $\nu(s)$ to the output $z(s)$.

In the case of a collocated actuator and sensor, $\mathbf{n}_a = \mathbf{n}_s$ and $\mathbf{r}_a = \mathbf{r}_s$, and hence $\psi_{a,\alpha} = \psi_{s,\alpha}$. This yields $C_\alpha \geq 0$ in Eq. (11), and it is straightforward to show that each modal contribution to the transfer function is positive-real and hence so is a sum of such terms. It is clear that the passivity property is independent of the specific values of the natural frequencies, damping ratios (which may be zero in the limiting case where $\mathcal{D} = \mathbf{0}$), eigenfunctions, and the number of terms in the modal expansion, and it hinges only on the collocation property [11].

An alternative approach to demonstrate passivity is to consider the energy

$$E(t) = \frac{1}{2} \int_V \dot{\mathbf{w}}^T \mathcal{M} \dot{\mathbf{w}} \, dV + \frac{1}{2} \int_V \mathbf{w}^T \mathcal{K} \mathbf{w} \, dV \geq 0 \quad (12)$$

It follows using this in conjunction with the PDE and sensor equations that

$$\dot{E} = \int_V \dot{\mathbf{w}}^T (\mathcal{M} \ddot{\mathbf{w}} + \mathcal{K} \mathbf{w}) \, dV \quad (13)$$

$$= - \int_V \dot{\mathbf{w}}^T \mathcal{D} \dot{\mathbf{w}} \, dV + \mathbf{n}_a^T \dot{\mathbf{w}}(\mathbf{r}_a, t) \nu(t)$$

$$= - \int_V \dot{\mathbf{w}}^T \mathcal{D} \dot{\mathbf{w}} \, dV + z(t) \nu(t) \quad (14)$$

in the collocated case. Integrating over the interval $[0, T]$ produces

$$\int_0^T z(t)\nu(t) dt = E(T) - E(0) + \int_0^T \int_V \dot{\mathbf{w}}^T \mathcal{D}\dot{\mathbf{w}} dV dt \geq \beta = -E(0) \tag{15}$$

which is a statement of passivity. This analysis is readily extended to multiple actuators and sensors and does not rely on the ability of the damping operator to be diagonalized by the undamped mode shapes. Hence, flexible mechanical structures with collocated force actuators and linear velocity sensors are passive systems, which are relatively easy to stabilize on the basis of the passivity theorem. It is useful to note that the simplest strictly passive negative feedback, $\nu(t) = -Kz(t)$ with $K > 0$, renders $\dot{E}(t) = -\int_V \dot{\mathbf{w}}^T \mathcal{D}\dot{\mathbf{w}} dV - Kz^2(t) \leq 0$ according to Eq. (14). The next section seeks to determine appropriate sensors and actuators for the Orr–Sommerfeld problem.

III. Orr–Sommerfeld Equation and Passivity Analysis

We consider a two-dimensional flow field occupying the region $(x, y) \in [0, \infty] \times [a, b]$ with a base parallel laminar flow $(U(y), 0)$ and associated pressure field $P(x, y)$. Assuming small perturbations $u(x, y, t)$, $v(x, y, t)$, and $p(x, y, t)$, the linearized incompressible Navier–Stokes equations [1] are

$$\frac{\partial u}{\partial x} + \frac{\partial v}{\partial y} = 0 \tag{16}$$

$$\frac{\partial u}{\partial t} + U \frac{\partial u}{\partial x} + U'v = -\frac{\partial p}{\partial x} + \frac{1}{Re} \left(\frac{\partial^2 u}{\partial x^2} + \frac{\partial^2 u}{\partial y^2} \right) \tag{17}$$

$$\frac{\partial v}{\partial t} + U \frac{\partial v}{\partial x} = -\frac{\partial p}{\partial y} + \frac{1}{Re} \left(\frac{\partial^2 v}{\partial x^2} + \frac{\partial^2 v}{\partial y^2} \right) \tag{18}$$

where $U'(y) = dU(y)/dy$. It has been assumed that quantities are nondimensionalized using the velocity U_0 and distance H . The Reynolds number is given by $Re = \rho U_0 H / \mu$, where ρ is the fluid density, and μ is the absolute viscosity. The boundary conditions are taken to be $u(x, a, t) = u(x, b, t) = v(x, b, t) = 0$, and the control variable is taken to be $v(x, a, t)$, which corresponds to wall-normal blowing and suction.

Let us introduce the stream function $\Psi(x, y, t)$, with the velocity components expressed in terms of it as

$$u = \frac{\partial \Psi}{\partial y}, \quad v = -\frac{\partial \Psi}{\partial x} \tag{19}$$

These satisfy Eq. (16) and, when substituted into Eqs. (17) and (18) while eliminating the pressure, yield

$$\nabla^2 \dot{\Psi} + (U\nabla^2 - U'') \frac{\partial \Psi}{\partial x} = \frac{1}{Re} \nabla^2 \nabla^2 \Psi \tag{20}$$

where ∇^2 is the Laplacian in x and y . This equation for the stream function was also developed in [3].

Introducing the spatial Fourier transform in the x direction, or alternatively letting

$$\Psi(x, y, t) = \Re e\{\phi(y, t) \exp(iax)\} \tag{21}$$

where $\phi(y, t)$ is the complex amplitude and α is the real wave number, leads to the Orr–Sommerfeld equation [1]:

$$-(D^2 - \alpha^2)\dot{\phi} + (Re)^{-1}(D^2 - \alpha^2)^2\phi + i\alpha[U''(y) - U(y)(D^2 - \alpha^2)]\phi = 0 \tag{22}$$

where $D\phi \equiv \partial\phi/\partial y$. The boundary conditions are $\phi_y(a, t) = \phi(b, t) = \phi_y(b, t) = 0$, and the (real) control inputs are $\nu(t) = [\Re e\{\phi(a, t)\} \Im m\{\phi(a, t)\}]^T = [\nu_r(t)\nu_i(t)]^T$; the vector ν should not

be confused with the scalar velocity components u and v . Noting that the velocity components satisfy

$$u(x, y, t) = \Re e\{D\phi(y, t) \exp(iax)\} \tag{23}$$

$$v(x, y, t) = -\Re e\{i\alpha\phi(y, t) \exp(iax)\} \tag{24}$$

we see that the control input ν can ultimately be related to the wall velocity $v_w(x, t) = v(x, a, t) = \alpha \Im m\{\phi(a, t)\} \cos \alpha x + \alpha \Re e\{\phi(a, t)\} \sin \alpha x$. This will be done in more detail in the following section. For now, we note that the control input provides additional boundary conditions for $\phi(a, t)$.

The energy is taken to be

$$E(t) = \frac{\alpha}{4\pi} \int_0^{2\pi/\alpha} \int_a^b (u^2 + v^2) dy dx = \frac{1}{2} \int_a^b (\phi_y^* \phi_y + \alpha^2 \phi^* \phi) dy \geq 0 \tag{25}$$

Note that the subscript notation $(\cdot)_y$ indicates the corresponding partial derivative; the superscript $(\cdot)^*$ denotes the complex conjugate. Taking the time derivative yields

$$\dot{E} = \frac{1}{2} \int_a^b (\dot{\phi}_y^* \phi_y + \phi_y^* \dot{\phi}_y + \alpha^2 \dot{\phi}^* \phi + \alpha^2 \phi^* \dot{\phi}) dy$$

Integrating the first two terms by parts and introducing the boundary conditions yields

$$\dot{E} = \frac{1}{2} \int_a^b \{\phi[-D^2 + \alpha^2]\dot{\phi}^* + \phi^*[-D^2 + \alpha^2]\dot{\phi}\} dy$$

which, after introducing the Orr–Sommerfeld equation and its complex conjugate, leads to

$$\begin{aligned} \dot{E} = & -\frac{1}{2} \int_a^b \phi\{[Re^{-1}(D^2 - \alpha^2)^2\phi^* + i\alpha\{U(y)(D^2 - \alpha^2) - U''(y)\}]\phi^*\} dy \\ & -\frac{1}{2} \int_a^b \phi^*\{[Re^{-1}(D^2 - \alpha^2)^2\phi - i\alpha\{U(y)(D^2 - \alpha^2) - U''(y)\}]\phi\} dy \end{aligned}$$

Integrating by parts the terms containing D^4 twice and the terms containing D^2 once while enforcing the boundary conditions yields

$$\begin{aligned} \dot{E} = & -Re^{-1} \left(\alpha^4 \int_a^b |\phi|^2 dy + 2\alpha^2 \int_a^b |D\phi|^2 dy + \int_a^b |D^2\phi|^2 dy \right) \\ & - \alpha \int_a^b U'(y) \Im m[\phi\phi_y^*] dy + Re^{-1} \Re e[\phi^* D^3\phi]_{y=a} \end{aligned} \tag{26}$$

Now, note that the last term in Eq. (26) can be written as

$$Re^{-1} \Re e[\phi^* D^3\phi]_{y=a} = Re^{-1} [\Re e\{D^3\phi(a, t)\} \Re e\{\phi(a, t)\} + \Im m\{D^3\phi(a, t)\} \Im m\{\phi(a, t)\}]$$

When an analogy is made between the placement of this term in Eq. (26) and that of the term $z(t)\nu(t)$ in Eq. (14), the observation is defined to be $z(t) = [\Re e\{D^3\phi(a, t)\} \Im m\{D^3\phi(a, t)\}]^T = [z_r(t)z_i(t)]^T$. At this stage, the output z is strictly a mathematical notion, but it will be related to physically measurable pressure quantities in the next section. For now, we note that, by comparison of this choice with the streamwise velocity perturbation in Eq. (23), it can be related to the second spatial derivative (normal direction) of this quantity at the wall.

Now, noting that $\Re e[\phi^* D^3\phi]_{y=a} = z^T(t)\nu(t)$, while integrating Eq. (26) with respect to time, yields

$$\int_0^T \mathbf{z}^T \boldsymbol{\nu} dt = \int_0^T \left(\alpha^4 \int_a^b |\phi|^2 dy + 2\alpha^2 \int_a^b |D\phi|^2 dy + \int_a^b |D^2\phi|^2 dy \right) dt + Re E(T) + \alpha Re \int_0^T \int_a^b U'(y) \Im m[\phi\phi_y^*] dy dt - Re E(0) \tag{27}$$

Clearly, the first term on the right-hand side and $E(T)$ are nonnegative. However, the third term containing the Reynolds number is indefinite and, potentially, destroys the passivity of the mapping from the input $\boldsymbol{\nu}$ to the output \mathbf{z} . In the absence of this term, the mapping is passive. However, there are still stabilizing influences to be had using this sensor/actuator pair. For example, using the simplest strictly passive output feedback law

$$\boldsymbol{\nu}(t) = -\bar{K}\mathbf{z}(t), \quad \bar{K} > 0 \tag{28}$$

may lead to a passive (closed-loop) system. Introducing it into Eq. (26) yields

$$\dot{E} = -Re^{-1} \left(\alpha^4 \int_a^b |\phi|^2 dy + 2\alpha^2 \int_a^b |D\phi|^2 dy + \int_a^b |D^2\phi|^2 dy \right) - Re^{-1} \bar{K} \mathbf{z}^T \mathbf{z} - \alpha \int_a^b U'(y) \Im m[\phi\phi_y^*] dy \tag{29}$$

which demonstrates the potential of the output feedback law to lead to an energy-dissipative closed-loop system if the two terms containing Re^{-1} are able to dominate the last term.

A. Realization of the Special Output Using Pressure Measurements

We would now like to relate the input/output pair $[\boldsymbol{\nu}, \mathbf{z}]$ to more physically meaningful quantities. The wall-normal velocity satisfies

$$v_w(x, t) = v(x, a, t) = -\Re e\{i\alpha\phi(a, t) \exp(i\alpha x)\} \tag{30}$$

$$= \alpha \Im m\{\phi(a, t)\} \cos \alpha x + \alpha \Re e\{\phi(a, t)\} \sin \alpha x \tag{31}$$

$$= \bar{v}_r(t) \cos \alpha x - \bar{v}_i(t) \sin \alpha x$$

where the following quantities have been defined:

$$\bar{v}_r(t) = \alpha \Im m\{\phi(a, t)\} = \alpha v_i(t) = v_w(0, t)$$

$$\bar{v}_i(t) = -\alpha \Re e\{\phi(a, t)\} = -\alpha v_r(t) = v_w(3\pi/(2\alpha), t)$$

The corresponding sensed variables are defined to be

$$\begin{aligned} \bar{z}_r(t) &= \Im m\{\phi_{yyy}(a, t)\}/\alpha = z_i(t)/\alpha, \\ \bar{z}_i(t) &= -\Re e\{\phi_{yyy}(a, t)\}/\alpha = -z_r(t)/\alpha \end{aligned} \tag{32}$$

and we note that $\mathbf{z}^T \boldsymbol{\nu} = \bar{\mathbf{z}}^T \bar{\boldsymbol{\nu}}$, where $\bar{\boldsymbol{\nu}} = [\bar{v}_r \ \bar{v}_i]^T$ and $\bar{\mathbf{z}} = [\bar{z}_r \ \bar{z}_i]^T$.

Because by Eq. (23) $u_{yy}(x, a, t) = \Re e\{i\phi_{yyy}(a, t)\} \cos \alpha x - \Im m\{\phi_{yyy}(a, t)\} \sin \alpha x$, it is readily shown that

$$\bar{z}_i(t) = \frac{1}{2} \int_{\pi/(2\alpha)}^{3\pi/(2\alpha)} u_{yy}(x, a, t) dx \tag{33}$$

$$\bar{z}_r(t) = -\frac{1}{2} \int_0^{\pi/\alpha} u_{yy}(x, a, t) dx \tag{34}$$

Now, considering the x component of the linearized Navier–Stokes equation in Eq. (17) and evaluating it at the lower wall ($x = a$)

while applying the boundary conditions $u(x, a, t) = u_x(x, a, t) = u_r(x, a, t) = 0$ gives

$$U'(a)v(x, a, t) + \frac{\partial p(x, a, t)}{\partial x} = \frac{1}{Re} u_{yy}(x, a, t) \tag{35}$$

Integrating both sides gives

$$\int_{x_1}^{x_2} u_{yy}(x, a, t) dx = Re \left\{ p(x_2, a, t) - p(x_1, a, t) + U'(a) \int_{x_1}^{x_2} v(x, a, t) dx \right\} \tag{36}$$

Setting $x_1 = \pi/\alpha$ and $x_2 = 0$ and using Eq. (34) gives

$$\bar{z}_r(t) = \frac{Re}{2} [p(0, a, t) - p(\pi/\alpha, a, t)] + \frac{Re U'(a)}{\alpha} \bar{v}_i(t) \tag{37}$$

Setting $x_1 = \pi/(2\alpha)$ and $x_2 = 3\pi/(2\alpha)$ and using Eq. (33) gives

$$\bar{z}_i(t) = \frac{Re}{2} [p(3\pi/(2\alpha), a, t) - p(\pi/(2\alpha), a, t)] - \frac{Re U'(a)}{\alpha} \bar{v}_r(t) \tag{38}$$

Columnnizing the two results produces

$$\bar{\mathbf{z}}(t) = \frac{Re}{2} \Delta \mathbf{p}(t) + \mathbf{Q} \bar{\boldsymbol{\nu}}(t) \tag{39}$$

where

$$\begin{aligned} \Delta \mathbf{p} &= \begin{bmatrix} p(0, a, t) - p(\pi/\alpha, a, t) \\ p(3\pi/(2\alpha), a, t) - p(\pi/(2\alpha), a, t) \end{bmatrix}, \\ \mathbf{Q} &= \frac{Re U'(a)}{\alpha} \begin{bmatrix} 0 & 1 \\ -1 & 0 \end{bmatrix} \end{aligned} \tag{40}$$

Introducing the output feedback law

$$\bar{\boldsymbol{\nu}}(t) = -\bar{K} \bar{\mathbf{z}}(t) \tag{41}$$

in Eq. (39) yields a feedback law using pressure measurements along the wall:

$$\bar{\boldsymbol{\nu}}(t) = -\frac{K Re}{2} (\mathbf{I} + \mathbf{K} \mathbf{Q})^{-1} \Delta \mathbf{p}(t) \tag{42}$$

Comparing the feedback law in Eq. (41) with that in Eq. (28), while noting $\bar{v}_r(t) = \alpha v_i(t)$, $\bar{v}_i(t) = -\alpha v_r(t)$, $\bar{z}_r(t) = z_i(t)/\alpha$, and $\bar{z}_i(t) = -z_r(t)/\alpha$, reveals that $\bar{K} = K/\alpha^2$, or $\boldsymbol{\nu}(t) = -(K/\alpha^2) \mathbf{z}(t)$, for the proposed controller. This is the simplest way to implement the control law mathematically. Physically, we note that, at each wave number, four pressure measurements are required on the wall at the locations $x_{s,j} = (j - 1)\pi/(2\alpha)$, $j = 1, 2, 3, 4$, as per Eqs. (39) and (40). The physical feedback law is Eq. (42).

In the remainder of the paper, we shall examine two wall-bounded parallel shear flows: the two-dimensional Poiseuille channel flow, and the two-dimensional Blasius boundary-layer flow. One of our objectives is to compare the two flows from the point of view of feedback stabilization using the input/output pair developed previously and examine the possibility of rendering the closed-loop system passive.

B. Poiseuille Flow

The Poiseuille flow is depicted in Fig. 3. The half-channel width is H , and the flow velocity at the midline ($y = 0$) is U_0 . The nominal

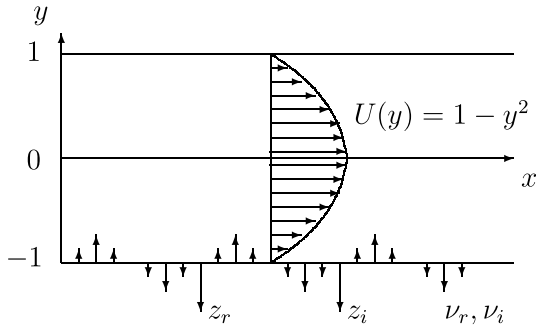


Fig. 3 Poiseuille flow.

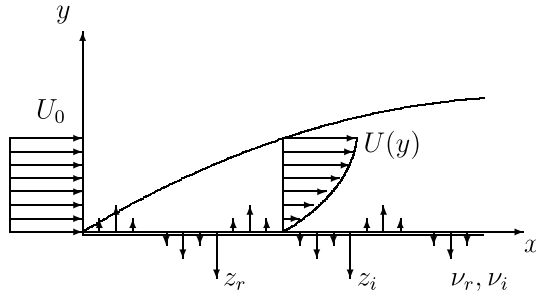


Fig. 4 Blasius boundary layer.

nondimensionalized flow velocity is $U(y) = 1 - y^2$. The upper and lower boundaries correspond to $a = -1$ and $b = 1$, with boundary conditions as discussed in the previous section.

C. Blasius Boundary Layer

The Blasius boundary layer [16] is depicted in Fig. 4. Although the nominal laminar flow (U, V) is known to be nonparallel ($V \neq 0$), we shall make the approximation $V = 0$ and take $U(y)$ to be the Blasius solution: $U(y) = df(\eta)/d\eta$, where $\eta = y_d \sqrt{\rho U_0 / (\mu x_d)} = 1.7207876573y$ (x_d and y_d refer to dimensional coordinates), and $f(\eta)$ is the solution of $2d^3f/d\eta^3 + (d^2f/d\eta^2)f = 0$, with $df(0)/d\eta = f(0) = 0$ and $d^2f(0)/d\eta^2 = 0.33205733622$, which yields the correct asymptotic boundary condition $df(\eta)/d\eta = 1$ as $\eta \rightarrow \infty$. The displacement thickness is given by $H = \delta^* = 1.7207876573 \sqrt{\mu x_d / (\rho U_0)}$, where the freestream velocity is U_0 . The local Reynolds number will be denoted by $Re = \rho U_0 \delta^* / \mu$, and δ^* will nondimensionalize length. Although $b \rightarrow \infty$, we will use a finite computational domain with $b = (16/H) \sqrt{\mu x_d / (\rho U_0)}$ (dimensionless), and at this boundary, we will impose the inviscid asymptotic solution $\phi_y(b, t) = -\alpha\phi(b, t)$, corresponding to the fact that $\phi \propto \exp(-\alpha y)$ as $y \rightarrow \infty$.

IV. Spatial Discretization Using Finite Elements

It is assumed that the y domain $[a, b]$ is broken into N_e equally sized finite elements (width ℓ), with the value of y at the nodes (element boundaries) denoted by $y_j = (j - 1)\ell, j = 1, \dots, N_e + 1$, where $\ell = (b - a)/N_e$. Let us denote the value of ϕ and its derivative at the nodes by $\phi_j(t) = \phi(y_j, t)$ and $\phi'_j(t) = \phi_y(y_j, t)$. Within the j th element, the following trial solution is assumed:

where $y = (j - 1 + \hat{y})\ell$, and \hat{y} is a local element coordinate system with $0 \leq \hat{y} \leq 1$. This element description was used in [12] in the case of Poiseuille flow. Our application to the Blasius flow and the controlled Orr–Sommerfeld equation is novel.

Based on Eq. (43), the finite element description of the Orr–Sommerfeld solution is given by

$$\phi(y, t) = \sum_{j=1}^{N_e} \Phi_j(y) \mathbf{q}^{(j)}(t) \tag{44}$$

where

$$\Phi_j(y) = \begin{cases} \mathbf{Y}^T(\hat{y})\mathbf{L}, & (j - 1)\ell \leq y \leq j\ell \\ \mathbf{0}, & \text{otherwise} \end{cases} \tag{45}$$

In preparation for a weak (variational) solution of the problem, we introduce a variation

$$\delta\phi(y, t) = \sum_{j=1}^{N_e} \Phi_j(y) \delta\mathbf{q}^{(j)}(t) \tag{46}$$

satisfying the boundary conditions

$$\delta\phi(a, t) = \delta\phi'(a, t) = 0, \quad \delta\phi(b, t) = \delta\phi'(b, t) = 0 \tag{47}$$

for the Poiseuille problem. In the case of the Blasius boundary layer, the boundary conditions at $y = b$ are not applied. Instead, we opt to enforce the conditions $\phi'(b, t) = -\alpha\phi(b, t)$ and $\delta\phi'(b, t) = -\alpha\delta\phi(b, t)$, which correspond to the inviscid asymptotic solution of the Orr–Sommerfeld equation, $\phi(y, t) \propto e^{-\alpha y}$.

Premultiplying the Orr–Sommerfeld equation in Eq. (22) by $\delta\phi$ and integrating by parts (from $y = a$ to $y = b$) yields

$$\begin{aligned} & \int_a^b [\alpha^2 \delta\phi \dot{\phi} + D(\delta\phi)D\dot{\phi}] dy - \delta\phi D\dot{\phi}|_{y=b} \\ & + \frac{1}{Re} \int_a^b [D^2(\delta\phi)D^2\phi + 2\alpha^2 D(\delta\phi)D\phi + \alpha^4 \delta\phi\phi] dy \\ & + \frac{1}{Re} [\delta\phi D^3\phi - D(\delta\phi)D^2\phi - 2\alpha^2 \delta\phi D\phi]|_{y=b} \\ & + i\alpha \int_a^b [\alpha^2 U(y)\delta\phi\phi + U''(y)\delta\phi\phi + U(y)D(\delta\phi)D\phi \\ & + U'(y)\delta\phi D\phi] dy - i\alpha U(y)\delta\phi D\phi \Big|_{y=b} = 0 \end{aligned} \tag{48}$$

where it has been observed that $\delta\phi(a, t) = \delta\phi_y(a, t) = 0$ because these quantities are prescribed. Substituting Eqs. (44) and (46) into Eq. (48) yields

$$\sum_{j=1}^{N_e} \delta\mathbf{q}^{(j)T} [\mathbf{M}_{r,j} \dot{\mathbf{q}}_j + (\mathbf{K}_{r,j} + i\mathbf{K}_{i,j}) \mathbf{q}^{(j)}] = 0 \tag{49}$$

where

$$\phi(y, t) = [1 \quad \hat{y} \quad \hat{y}^2 \quad \hat{y}^3] \begin{bmatrix} 1 & 0 & 0 & 0 \\ 0 & \ell & 0 & 0 \\ -3 & -2\ell & 3 & -\ell \\ 2 & \ell & -2 & \ell \end{bmatrix} [\phi_j(t) \phi'_j(t) \phi_{j+1}(t) \phi'_{j+1}(t)]^T = \mathbf{Y}^T(\hat{y})\mathbf{L}\mathbf{q}^{(j)}(t) \tag{43}$$

$$\begin{aligned}
 M_{r,j} &= L^T \int_0^1 \left[\alpha^2 Y(\hat{y}) Y^T(\hat{y}) + \frac{1}{\ell^2} \frac{d}{d\hat{y}} Y(\hat{y}) \frac{d}{d\hat{y}} Y^T(\hat{y}) \right] d\hat{y} L \\
 K_{r,j} &= \frac{1}{Re} L^T \int_0^1 \left[\alpha^4 Y(\hat{y}) Y^T(\hat{y}) + 2\alpha^2 \frac{1}{\ell^2} \frac{d}{d\hat{y}} Y(\hat{y}) \frac{d}{d\hat{y}} Y^T(\hat{y}) \right. \\
 &\quad \left. + \frac{1}{\ell^4} \frac{d^2}{d\hat{y}^2} Y(\hat{y}) \frac{d^2}{d\hat{y}^2} Y^T(\hat{y}) \right] d\hat{y} L \\
 K_{i,j} &= \alpha L^T \int_0^1 \left\{ [(\alpha^2 U((j-1) + \hat{y}) \ell) + U''((j-1) + \hat{y}) \ell] Y(\hat{y}) Y^T(\hat{y}) \right. \\
 &\quad + U((j-1) + \hat{y}) \ell \frac{1}{\ell^2} \frac{d}{d\hat{y}} Y(\hat{y}) \frac{d}{d\hat{y}} Y^T(\hat{y}) \\
 &\quad \left. + \frac{1}{\ell} U'((j-1) + \hat{y}) \ell Y(\hat{y}) \frac{d}{d\hat{y}} Y^T(\hat{y}) \right\} d\hat{y} L
 \end{aligned}$$

In the Poiseuille case, the terms evaluated at $y = b$ in Eq. (48) are zero. In the Blasius case, they add additional terms to the matrices M_{r,N_e} , K_{r,N_e} , and K_{i,N_e} .

Defining $\hat{q} = [\phi_1 \phi'_1 \dots \phi_{N_e+1} \phi'_{N_e+1}]^T$ with the corresponding definition for $\delta\hat{q}$, Eq. (49) can be written as

$$\delta\hat{q}^T [\hat{M}_r \hat{q} + (\hat{K}_r + i\hat{K}_i) \hat{q}] = 0 \tag{50}$$

where the global matrices \hat{M}_r , \hat{K}_r , and \hat{K}_i are assembled from their elemental counterparts using the usual procedures of the finite element method. Because the left-hand side of Eq. (50) must vanish for all variations $\delta\hat{q}$, we arrive at

$$\hat{M}_r \hat{q} + (\hat{K}_r + i\hat{K}_i) \hat{q} = 0 \tag{51}$$

and we momentarily ignore the rows corresponding to $\delta q_j = 0$.

The boundary conditions are now applied by setting $\phi'_1 = 0$ and taking the terms involving ϕ_1 to the right-hand side of the equation to form the control input. In the Poiseuille case, we also set $\phi_{N_e+1} = \phi'_{N_e+1} = 0$. In the Blasius case, we set $\phi'_{N_e+1} = -\alpha \phi_{N_e+1}$. Defining $q = [\phi_2 \phi'_2 \dots \phi_{N_e} \phi'_N \phi_{N_e+1}]^T$ (ϕ_{N_e+1} is omitted in the Poiseuille case) and removing the appropriate rows and columns from \hat{M}_r , \hat{K}_r , and \hat{K}_i yields

$$M_r \hat{q} + (K_r + iK_i) q = (B_{1r} + iB_{1i}) \phi_1 + B_{2r} \dot{\phi}_1 \tag{52}$$

where M_r , K_r , and K_i are the reduced matrices. In the Blasius case, additional terms are added to the last row and last column of each matrix on the left-hand side to enforce $\phi'_{N_e+1} = -\alpha \phi_{N_e+1}$. It is straightforward to form B_{1r} from the (3,1) and (4,1) entries of \hat{K}_r , B_{1i} from the (3,1) and (4,1) entries of \hat{K}_i , and B_{2r} from the (3,1) and (4,1) entries of \hat{M}_r .

Defining the (real) state vector to be $\hat{x} = [q_r^T q_i^T]^T$, where $q_r = \Re e\{q\}$ and $q_i = \Im m\{q\}$, and defining the control input to be $\nu = [\Re e\{\phi_1\} \Im m\{\phi_1\}]^T$, the state-space model can be written as

$$\dot{\hat{x}} = A\hat{x} + \hat{B}_1 \nu + \hat{B}_2 \dot{\nu} \tag{53}$$

$$z = C\hat{x} + \hat{D}\nu \tag{54}$$

where

$$\begin{aligned}
 A &= \begin{bmatrix} -M_r^{-1} K_r & M_r^{-1} K_i \\ -M_r^{-1} K_i & -M_r^{-1} K_r \end{bmatrix}, \\
 \hat{B}_1 &= \begin{bmatrix} M_r^{-1} B_{1r} & -M_r^{-1} B_{1i} \\ M_r^{-1} B_{1i} & M_r^{-1} B_{1r} \end{bmatrix}, \\
 \hat{B}_2 &= \begin{bmatrix} M_r^{-1} B_{2r} & \mathbf{0} \\ \mathbf{0} & M_r^{-1} B_{2r} \end{bmatrix}
 \end{aligned}$$

The (real) output is taken to be $z(t) = [\Re e\{\phi_{yy}(a, t)\} \Im m\{\phi_{yy}(a, t)\}]^T$ so that C and \hat{D} can be easily

formed by taking three derivatives of the trial solution in Eq. (44). In particular, $\hat{D} = \text{diag}\{12/\ell^3, 12/\ell^3\}$. The term containing $\dot{\nu}$ can be removed by defining a new state vector $x = \hat{x} - \hat{B}_2 \nu$. The ensuing state description is

$$\dot{x} = Ax + B\nu, \quad B = \hat{B}_1 + A\hat{B}_2 \tag{55}$$

$$z = Cx + D\nu, \quad D = \hat{D} + C\hat{B}_2 \tag{56}$$

State-space models of the Orr–Sommerfeld equation are discussed in [17]. Our use of the finite element method in this regard has several advantages. Chief among these are the physically meaningful nature of the elements of q and the presence of the control inputs as nodal degrees of freedom.

V. Stability Analysis

On the basis of the previous passivity analysis, the following output feedback is now considered:

$$\nu(t) = -\bar{K}z(t) + d(t), \quad \bar{K} = K/\alpha^2 \tag{57}$$

which is a strictly passive negative feedback. The input $d(t)$ corresponds to the exogenous input in Fig. 1. Wrapping this around the system in Eqs. (55) and (56) produces the closed-loop system

$$\dot{x} = \bar{A}x + \bar{B}d, \quad \bar{A} = A - B(I + \bar{K}D)^{-1} \bar{K}C, \quad \bar{B} = B(I + \bar{K}D)^{-1} \tag{58}$$

$$z = \bar{C}x + \bar{D}d, \quad \bar{C} = C - D(I + \bar{K}D)^{-1} \bar{K}C, \quad \bar{D} = D(I + \bar{K}D)^{-1} \tag{59}$$

with corresponding transfer function matrix $\bar{G}(s) = \bar{C}(sI - \bar{A})^{-1} \bar{B} + \bar{D}$, where $z(s) = \bar{G}(s)d(s)$. In the numerical examples to follow, $N_e = 240$ finite elements are employed.

A. Poiseuille Case

The eigenvalues of \bar{A} (the closed-loop system poles) clearly depend on \bar{K} . We begin with the open-loop case, $K = \bar{K} = 0$ so that $\bar{A} = A$. The first 10 eigenvalues of A (with smallest positive imaginary parts) are given in Table 1 for $Re = 2000$ and $\alpha = 1$. There, they are compared with the results of [18], which used an expansion in Chebyshev polynomials to discretize the Orr–Sommerfeld equation. There is agreement to six significant figures in all cases.

The eigenvalues of \bar{A} for $0 \leq K < \infty$ are graphically depicted in the root locus plot in Fig. 5. The root locus plot considers the classic case of $Re = 10,000$ and $\alpha = 1$ used by [3,19]. For $K = 0$, the eigenvalues are the open-loop poles and are depicted by the symbol X . The system is unstable at this Reynolds number and wave number because there are poles located in the right half-plane at

Table 1 Orr–Sommerfeld eigenvalues for Poiseuille case, $Re = 2000$, $\alpha = 1$

Schmid and Henningson [18]		Damaren ($N_e = 240$)	
$\Re e\{\lambda/\alpha\}$	$\Im m\{\lambda/\alpha\}$	$\Re e\{\lambda/\alpha\}$	$\Im m\{\lambda/\alpha\}$
-0.01979866	0.31210030	-0.01979863	0.31210026
-0.07671992	0.42418427	-0.07671979	0.42418411
-0.07804706	0.92078667	-0.07804705	0.92078666
-0.07820060	0.92091806	-0.07820059	0.92091805
-0.13990151	0.85717055	-0.13990146	0.85717051
-0.14031674	0.85758968	-0.14031669	0.85758963
-0.20190508	0.79399812	-0.20190490	0.79399800
-0.20232063	0.79413424	-0.20232049	0.79413410
-0.22134137	0.63912513	-0.22134066	0.63912471
-0.22356175	0.53442105	-0.22356121	0.53442090

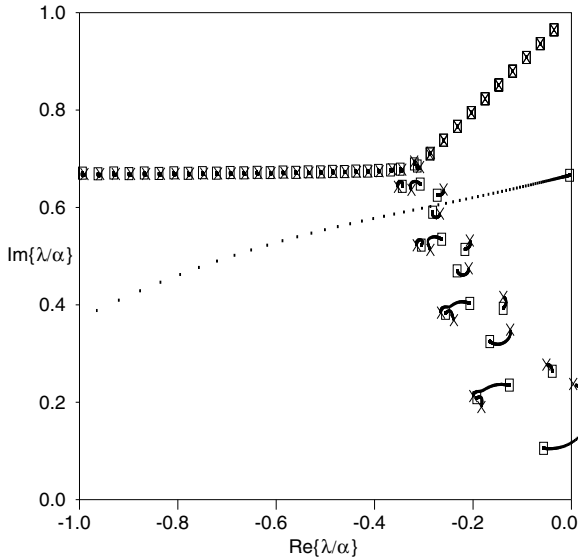


Fig. 5 Root locus plot for Poiseuille flow ($Re = 10,000$, $\alpha = 1.0$; \times : open-loop poles, squares: open-loop zeros, solid line: locus of closed-loop poles).

$\lambda/\alpha = 0.00373973 \pm i0.2375259$. This compares with Orszag’s value of $\lambda/\alpha = 0.00373967 \pm i0.2375265$. As $K \rightarrow \infty$, the closed-loop eigenvalues tend toward the system open-loop zeros, which are the eigenvalues of $A - BD^{-1}C$ (they are indicated by squares). This follows from that fact that $\tilde{A} \rightarrow A - BD^{-1}C$ as $K \rightarrow \infty$ in Eq. (58). In the present case, the system is minimum-phase because all of the zeros lie in the left half-plane, although there is a pair of zeros close to the imaginary axis at $\lambda/\alpha = -0.003571 \pm i0.666043$. The dotted line corresponds to a locus of closed-loop poles that starts off the left side of the plot and converges almost to the imaginary axis at high gain. Also, note the pole-zero cancellations associated with the line of poles and zeros along the line $\Im m\{\lambda\}/\alpha = 0.67$, which ultimately heads toward $\lambda = i1$. The cancellations are associated with the fact that these modes are uncontrollable or unobservable or both from the wall-based sensing and actuation as discussed in [8].

Stability diagrams for various values of K are given in Fig. 6. These diagrams consider the stability of (Re, α) pairs for a given value of K . For lower values of K , the size of the instability region is larger than the open-loop case. However, for $K = 0.01$, the entire depicted region is stable for all (Re, α) pairs using this single gain value. Note that the root loci in Fig. 5 are consistent with Fig. 6 (i.e., at small gain, the feedback makes things worse, consistent with a nonpassive system).

B. Blasius Case

In the case of the Blasius boundary-layer flow, the open-loop eigenvalues are given in Table 2 for $Re = 800$ (based on displacement thickness) and $\alpha = 1$. They are compared with those of [18], which used Chebyshev polynomials, but the handling of the boundary condition at infinity was not clear. There is agreement to four significant figures with the discrepancy probably due to the approximate nature of our use of the inviscid boundary condition at a finite upper boundary.

The root locus plot is given in Fig. 7 for the case of $Re = 998$, $\alpha = 0.308$ considered by [20]. In the open-loop case, there are unstable eigenvalues at $\lambda/\alpha = 0.007933 \pm i0.364115$, which agrees well with those obtained by [20], $\lambda/\alpha = 0.0079 \pm i0.3641$, and those obtained by [21], $\lambda/\alpha = 0.007960 \pm i0.364123$. Interestingly, our results show that there are unstable zeros very close to these values (the zeros are located at $\lambda/\alpha = 0.001968 \pm i0.360180$); hence, the Blasius flow for this case is nonminimum-phase. Once again, the dotted line corresponds to a locus of closed-loop poles that starts off the left side of the plot and converges almost to the imaginary axis at high gain.

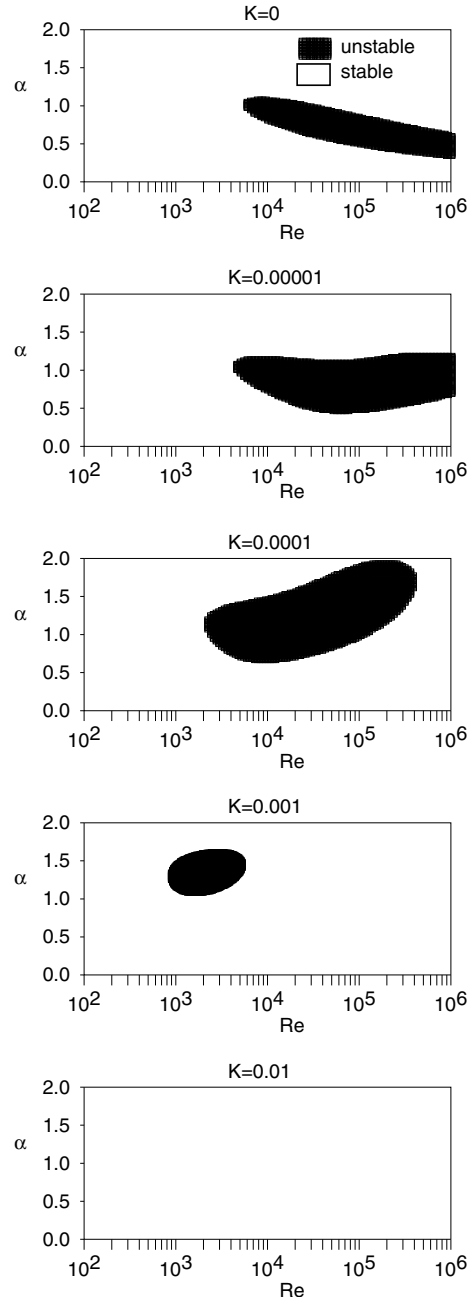


Fig. 6 Stability diagrams for Poiseuille flow.

The high-frequency line of poles and zeros (roughly along the line $\lambda/\alpha = i1$) is an approximation to the continuous spectrum, which arises due to the semi-infinite domain. Our finite computational

Table 2 Orr–Sommerfeld eigenvalues for Blasius case, $Re = 800$, $\alpha = 1$

Schmid and Henningson [18]		Damaren ($N_e = 240$)	
$\Re e\{\lambda/\alpha\}$	$\Im m\{\lambda/\alpha\}$	$\Re e\{\lambda/\alpha\}$	$\Im m\{\lambda/\alpha\}$
-0.08240950	0.29440241	-0.08239432	0.29438052
-0.16979273	0.46408909	-0.16975992	0.46402206
-0.21355653	0.58341130	-0.21357389	0.58337109
-0.21441674	0.23752687	-0.21439803	0.23752579
-0.28694526	0.67030439	-0.28682292	0.67030004
-0.29556202	0.42182040	-0.29550007	0.42181289
-0.35409567	0.78475538	-0.35410324	0.78465371
-0.35864989	0.57920596	-0.35852178	0.57917397
-0.40824449	0.72486516	-0.40802471	0.72477547

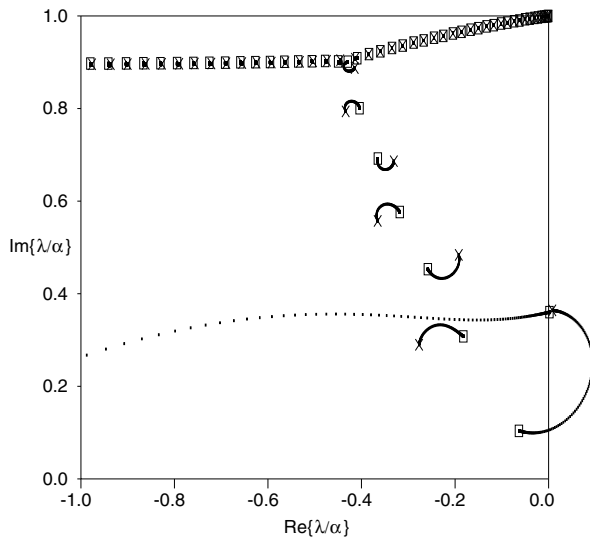


Fig. 7 Root locus plot for Blasius flow ($Re = 998$, $\alpha = 0.308$; \times : open-loop poles, squares: open-loop zeros, solid line: locus of closed-loop poles).

domain results in discrete eigenvalues. These eigenvalues can be compared with the exact continuous spectrum from [22]: $\lambda = -(1 + \gamma^2)(\alpha/Re) \pm i1 \pm -(1 + \gamma^2)(3.1 \times 10^{-4}) \pm i1$, $\gamma \in \mathfrak{R}$. In [22], it is stated that the corresponding eigenfunctions “are essentially freestream modes and do not penetrate very far into the boundary layer.” For this reason they have very poor controllability and observability with respect to the plate-mounted sensing and actuation, which leads to pole-zero cancellations. Our closest eigenvalue to the imaginary axis is located at $-5.5 \times 10^{-4} \pm i0.999995$, which can be compared to the preceding exact result. As the computational boundary at $y = b$ increases, the real part migrates toward the exact result.

Stability diagrams for various values of K are shown in Fig. 8. Initially, the instability region becomes larger, but at $K = 0.25$, the entire depicted region is stable. It should not be concluded that this is the case for larger values of K , which is expected given the occurrence of right half-plane zeros. Again, it is noted that the root locus plot is consistent with the stability diagrams (i.e., at small gain, the feedback makes things worse, consistent with a nonpassive system).

VI. Feedback Passivation

As shown in the previous section, the open-loop systems ($K = 0$) are not stable at all wave numbers and Reynolds numbers. Passive linear time-invariant systems must have poles in the closed left half-plane, which is clearly not the case for the unstable regions in Figs. 6 and 8. However, there exists the possibility that the closed-loop system described by Eqs. (58) and (59) is rendered passive by the output feedback. For systems with nonzero high-frequency gain ($D \neq \mathbf{0}$), the necessary and sufficient condition for this to be possible are $\text{Det } D \neq 0$ and $A - BD^{-1}C$ having eigenvalues with negative-real parts (i.e., the system is minimum-phase [23]).

A. Poiseuille Case

For the case of $Re = 10,000$, $\alpha = 1$, $K = 0.001$, the eigenvalues of the Hermitian part of $\tilde{G}(i\omega)$ are shown in Fig. 9 as a function of ω . This matrix is positive-definite for all frequencies, showing that the transfer matrix is positive-real (in fact, strictly positive-real), and hence the system is passive. It was verified that all (Re, α) pairs depicted in Fig. 6 for $K = 0.01$ enjoy this property.

B. Blasius Case

For the case of $Re = 998$, $\alpha = 0.308$, $K = 0.25$, the eigenvalues of the Hermitian part of $\tilde{G}(i\omega)$ are shown in Fig. 10 as a function of ω .

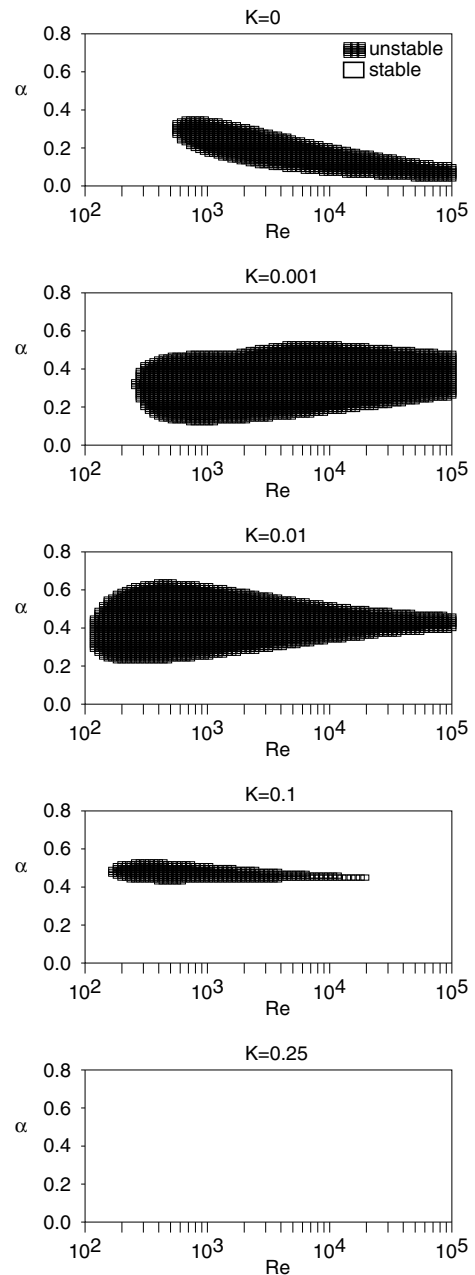


Fig. 8 Stability diagrams for Blasius flow.

This matrix is not positive-definite for all frequencies, showing that the transfer matrix is not positive-real, and hence the system is not passive. This is expected given the right half-plane zero in Fig. 7. A search for (Re, α) pairs that had a positive-real transfer matrix for $K = 0.25$ did not find any such pair.

Because our emphasis has been on the choice of inputs and outputs, it was decided to start with a simple controller design. Readers may wonder if there are other controller designs that can render the closed-loop transfer function matrix positive-real (hence a passive system). These are as follows: constant-gain output feedback but restricted to strictly proper plants (i.e., $D = \mathbf{0}$) [24]; linear dynamic compensators but restricted to strictly proper plants [25]; and linear dynamic compensators with no restriction to strictly proper plants [26]. It is unclear from these papers whether the problem can be solved for nonminimum-phase systems (like the Blasius case), but [24] shows that, if the problem for a strictly proper plant cannot be solved with constant output feedback, it cannot be solved using a dynamic compensator with proper controller transfer function matrix. If this result extends to proper plants (D not necessarily zero),

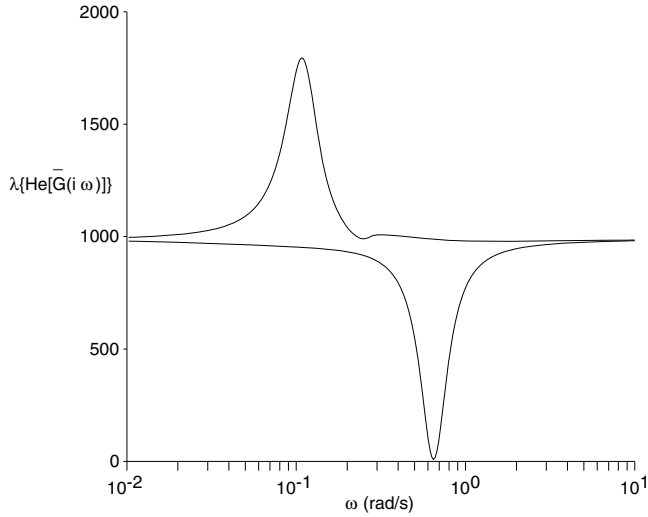


Fig. 9 Eigenvalues of the Hermitian part for Poiseuille flow; $Re = 10,000, \alpha = 1.0, K = 0.001$.

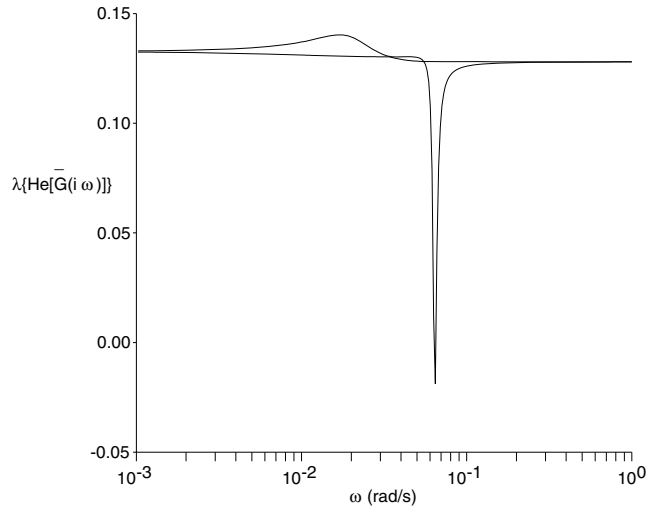


Fig. 10 Eigenvalues of the Hermitian part for Blasius flow; $Re = 998, \alpha = 0.308, K = 0.25$.

then the Blasius case cannot be made positive-real with any proper dynamic compensator.

VII. Time-Domain Simulations

This section shows results from simulating the behavior of the system defined by Eqs. (57–59). Taking the external disturbance $d = \mathbf{0}$ with nonzero initial conditions $\mathbf{x}(0)$ yields

$$\mathbf{x}(t) = \exp(\bar{A}t)\mathbf{x}(0) \tag{60}$$

$$\nu(t) = -\bar{K}\bar{C}\mathbf{x}(t) \tag{61}$$

The latter quantity can be used to evaluate the wall-normal velocity $v_w(\bar{x}, t)$ using Eq. (31), where we opt to evaluate it at $\bar{x} = \pi/(4\alpha)$. We will also determine the streamwise velocity perturbation $u(\bar{x}, y, t)$ using expression (23), where $y = -0.975$ for the Poiseuille example and $y = 0.344$ for the Blasius example. These locations are chosen because they produce the largest velocity magnitudes. The energy ratio $E(t)/E(0)$ is calculated using Eq. (25). It is readily shown using the results of Sec. IV that

$$E(t) = \frac{1}{2}\mathbf{x}^T(t)\mathbf{M}\mathbf{x}(t), \quad \mathbf{M} = \text{blockdiag}\{\mathbf{M}_r, \mathbf{M}_r\} \tag{62}$$

The initial conditions $\mathbf{x}(0)$ are chosen to provide the largest transient energy growth [27], i.e., to maximize the quantity

$$\begin{aligned} J &= \sup_{T \geq 0} \sup_{\mathbf{x}(0)} \left\{ \frac{E(T)}{E(0)} \right\} \\ &= \sup_{T \geq 0} \sup_{\mathbf{x}(0)} \left\{ \frac{\mathbf{x}^T(0) \exp(\bar{A}^T T) \mathbf{M} \exp(\bar{A} T) \mathbf{x}(0)}{\mathbf{x}^T(0) \mathbf{M} \mathbf{x}(0)} \right\} \end{aligned}$$

This leads to a generalized symmetric eigenproblem nested within a search over $T \geq 0$. The maximum eigenvalue for given T yields the maximum energy ratio $E(T)/E(0)$, and the eigenvector corresponding to it yields the optimal initial condition. The corresponding optimal perturbations $u_{\text{opt}}(y) = \epsilon u(\bar{x}, y, 0)$ and $v_{\text{opt}}(y) = \epsilon v(\bar{x}, y, 0)$ can be determined from the eigenvector $\mathbf{x}_{\text{opt}}(t)$ corresponding to the largest eigenvalue. It is assumed that the eigenvector is normalized to $(1/2)\mathbf{x}_{\text{opt}}^T \mathbf{M} \mathbf{x}_{\text{opt}} = 1$, and ϵ is a scaling. In the results to be presented, $\epsilon = 0.001$ for the Poiseuille case and $\epsilon = 0.01$ for the Blasius case. These were selected to yield maximum perturbations on the order of 1% of the maximum value of $U(y)$ (U_0). Note that when calculating velocities u and v , one must use the state vector $\hat{\mathbf{x}}(t) = \mathbf{x}(t) + \hat{\mathbf{B}}_2 \nu(t)$.

A. Poiseuille Case

For these simulation results, the following parameters were used: $Re = 10,000, \alpha = 1, K = 0.001$. The optimal perturbations are presented in Fig. 11. The energy ratio $E(t)/E(0)$, the wall-normal velocity $v_w(\bar{x}, t)$, and the streamwise perturbation velocity component $u(\bar{x}, -0.975, t)$ are given in Fig. 12. We note that the wall-normal velocity (the control input) is of the same order as the initial optimal perturbations. The time constant (time to half-amplitude) for the energy decay is $\tau \approx 7$.

B. Blasius Case

For these simulation results, the following parameters were used: $Re = 998, \alpha = 0.308, K = 0.05$. The optimal perturbations are presented in Fig. 13. Note that the dimensionless wall-normal

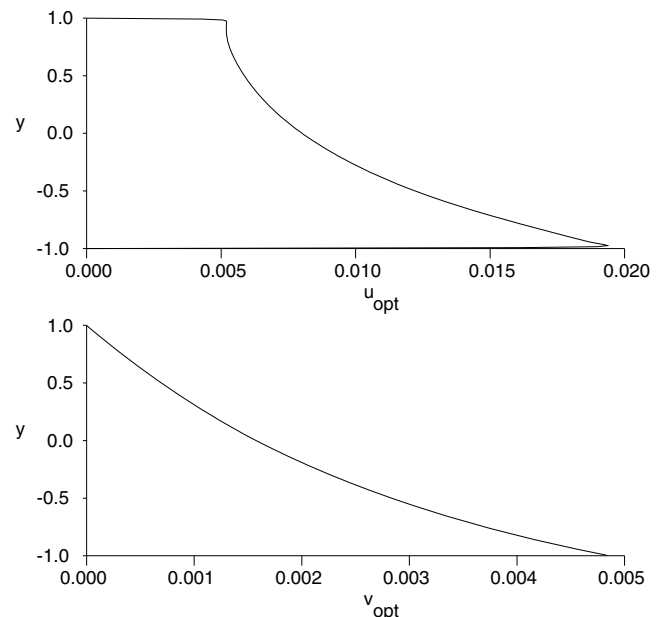


Fig. 11 Optimal perturbations for Poiseuille flow; $Re = 10,000, \alpha = 1, K = 0.001, \epsilon = 0.001$.

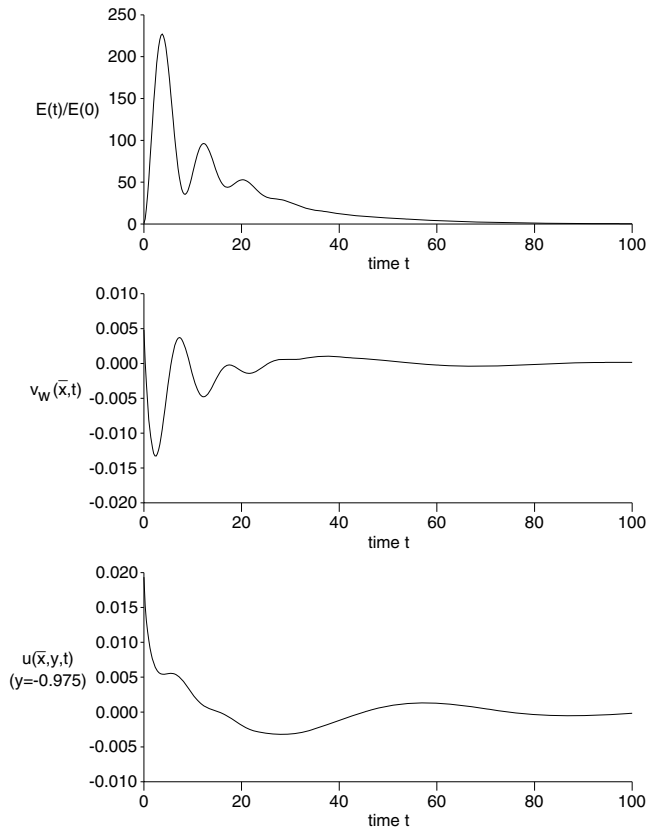


Fig. 12 Energy ratio, wall-normal velocity, and streamwise velocity perturbation for Poiseuille flow; $Re = 10,000$, $\alpha = 1$, $K = 0.001$, $\epsilon = 0.001$, $\bar{x} = \pi/(4\alpha)$.

coordinate y has been multiplied by 1.7207876573 so that it corresponds to the natural boundary-layer coordinate $\eta = y_d \sqrt{\rho U_0 / (\mu x_d)}$, which was introduced in Sec. III.C. The energy ratio $E(t)/E(0)$, the wall-normal velocity $v_w(\bar{x}, t)$, and the streamwise perturbation velocity component $u(\bar{x}, 0.344, t)$ are given in Fig. 14. We note that the wall-normal velocity is of the same order as the initial optimal perturbations. The time constant for the energy decay is $\tau \approx 20$.

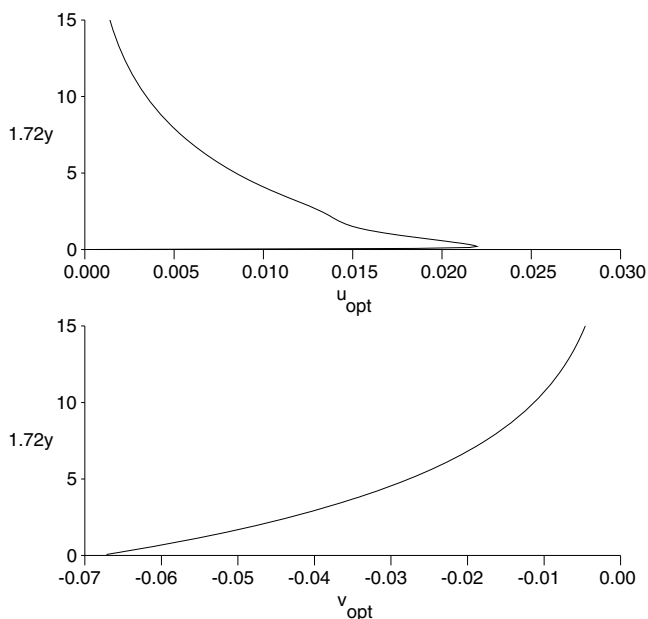


Fig. 13 Optimal perturbations for Blasius flow; $Re = 998$, $\alpha = 0.308$, $K = 0.05$, $\epsilon = 0.01$.

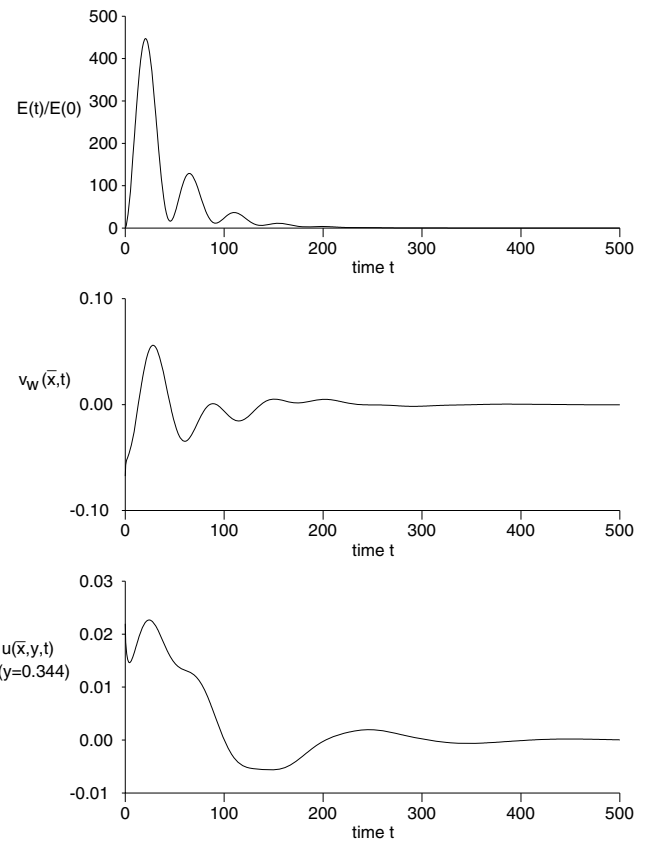


Fig. 14 Energy ratio, wall-normal velocity, and streamwise velocity perturbation for Blasius flow; $Re = 998$, $\alpha = 0.308$, $K = 0.05$, $\epsilon = 0.01$, $\bar{x} = \pi/(4\alpha)$.

VIII. Conclusions

The important property of passivity has been examined in the case of the boundary-feedback controlled Orr–Sommerfeld equation. A study of the work-energy balance was used to select the appropriate sensed variables corresponding to wall-normal velocity actuation. This corresponded to the second derivative (wall-normal direction) of the transverse velocity, which can be constructed from pressure measurements at judiciously chosen points along the wall. Although this choice of sensing and actuation did not lead to passivity in the open-loop case, it was demonstrated that a simple negative output feedback law produces a passive closed-loop system. This was shown to be true for the case of Poiseuille flow when the gain was sufficiently large. In the case of the Blasius boundary-layer base flow, the system was nonminimum-phase and hence could not be rendered passive by output feedback. However, for sufficiently large feedback gains (but not too large), the system is stabilized for a wide variety of Reynolds numbers and wave numbers using a single feedback gain. This is also true for Poiseuille flow.

References

- [1] Drazin, P. G., and Reid, W. H., *Hydrodynamic Stability*, Cambridge Univ. Press, Cambridge, England, U.K., 1981, Chap. 4. doi:10.1017/CBO9780511616938
- [2] Bewley, T. R., “Flow Control: New Challenges for a New Renaissance,” *Progress in Aerospace Sciences*, Vol. 37, No. 1, 2001, pp. 21–58. doi:10.1016/S0376-0421(00)00016-6
- [3] Joshi, S. S., Speyer, J. L., and Kim, J., “A Systems Theory Approach to the Feedback Stabilization of Infinitesimal and Finite-Amplitude Disturbances in Plane Poiseuille Flow,” *Journal of Fluid Mechanics*, Vol. 332, No. 2, 1997, pp. 157–184.
- [4] Bewley, T. R., and Liu, S., “Optimal and Robust Control and Estimation of Linear Paths to Transition,” *Journal of Fluid Mechanics*, Vol. 365, No. 6, 1998, pp. 305–349. doi:10.1017/S0022112098001281

- [5] Bagheri, S., Brandt, L., and Henningson, D. S., "Input-Output Analysis, Model Reduction, and Control of the Flat-Plate Boundary Layer," *Journal of Fluid Mechanics*, Vol. 620, No. 2, 2009, pp. 263–298.
doi:10.1017/S0022112008004394
- [6] Belson, B. A., Semeraro, O., Rowley, C. W., and Henningson, D. S., "Feedback Control of Instabilities in the Two-Dimensional Blasius Boundary Layer: The Role of Sensors and Actuators," *Physics of Fluids*, Vol. 25, No. 5, 2013, Paper 054106.
doi:10.1063/1.4804390
- [7] Butler, K. M., and Farrell, B. F., "Three-Dimensional Optimal Perturbations in Viscous Shear Flow," *Physics of Fluids A: Fluid Dynamics*, Vol. 4, No. 8, 1992, pp. 1637–1650.
doi:10.1063/1.858386
- [8] Kim, J., and Bewley, T. R., "A Linear Systems Approach to Flow Control," *Annual Review of Fluid Mechanics*, Vol. 39, 2007, pp. 383–417.
doi:10.1146/annurev.fluid.39.050905.110153
- [9] Desoer, C. A., and Vidyasagar, M., *Feedback Systems: Input-Output Properties*, Academic Press, New York, 1975, Chap. 6.
doi:10.1137/1.9780898719055.ch6
- [10] Youla, D. C., Castriota, L. J., and Carlin, H. J., "Bounded Real Scattering Matrices and the Foundations of Linear Passive Network Theory," *IRE Transactions on Circuit Theory*, Vol. 6, No. 1, 1959, pp. 102–124.
doi:10.1109/TCT.1959.1086518
- [11] Benhabib, R. J., Iwens, R. P., and Jackson, R. L., "Stability of Large Space Structure Control Systems Using Positivity Concepts," *Journal of Guidance, Control, and Dynamics*, Vol. 4, No. 5, 1981, pp. 487–494.
doi:10.2514/3.56100
- [12] Mamou, M., and Khalid, M., "Finite Element Solution of the Orr–Sommerfeld Equation Using High Precision Hermite Elements: Plane Poiseuille Flow," *International Journal for Numerical Methods in Fluids*, Vol. 44, No. 7, 2004, pp. 721–735.
doi:10.1002/(ISSN)1097-0363
- [13] Sharma, A. S., Morrison, J. F., McKeon, B. J., Limbeer, D. J. N., Koberg, W. H., and Kerwin, S. J., "Relaminarisation of Re $T = 100$ Globally Stabilising Linear Feedback Control," *Physics of Fluids*, Vol. 23, No. 12, 2011, Paper 125105.
doi:10.1063/1.3662449
- [14] Marquez, H. J., *Nonlinear Control Systems*, Wiley, Hoboken, NJ, 2003, Chap. 8.
- [15] Meirovitch, L., *Analytical Methods in Vibrations*, Macmillan, Toronto, ON, 1967, Chap. 5.
- [16] Schlichting, H., *Boundary-Layer Theory*, 7th ed., McGraw–Hill, New York, 1979, Chap. 7.
- [17] Or, A. C., Speyer, J. L., and Kim, J., "State-Space Approximations of the Orr–Sommerfeld System with Boundary Inputs and Outputs," *Journal of Guidance, Control, and Dynamics*, Vol. 33, No. 3, 2010, pp. 794–802.
doi:10.2514/1.46479
- [18] Schmid, P. J., and Henningson, D. S., *Stability and Transition in Shear Flows*, Springer–Verlag, 2001, Sec. A.7.
doi:10.1007/978-1-4613-0185-1
- [19] Orszag, S. A., "Accurate Solution of the Orr–Sommerfeld Stability Equation," *Journal of Fluid Mechanics*, Vol. 50, No. 4, 1971, pp. 689–703.
doi:10.1017/S0022112071002842
- [20] Jordinson, R., "Spectrum of Eigenvalues of the Orr–Sommerfeld Equation for Blasius Flow," *Physics of Fluids*, Vol. 14, No. 11, 1971, pp. 2535–2537.
doi:10.1063/1.1693363
- [21] Grosch, C. E., and Orszag, S. A., "Numerical Solution of Problems in Unbounded Regions: Coordinate Transforms," *Journal of Computational Physics*, Vol. 25, No. 3, 1977, pp. 273–295.
doi:10.1016/0021-9991(77)90102-4
- [22] Grosch, C. E., and Salwen, H., "The Continuous Spectrum of the Orr–Sommerfeld Equation. Part 1. The Spectrum and the Eigenfunctions," *Journal of Fluid Mechanics*, Vol. 87, No. 1, 1978, pp. 33–54.
doi:10.1017/S0022112078002918
- [23] Abdallah, C., Dorato, P., and Karni, S., "SPR Design Using Feedback," *Proceedings of the American Control Conference*, IEEE Publ., Piscataway, NJ, 1991, pp. 1742–1743.
- [24] Huang, C. H., Ioannou, P. A., Maroulas, J., and Safonov, M. G., "Design of Strictly Positive Real Systems Using Constant Output Feedback," *IEEE Transactions on Automatic Control*, Vol. 44, No. 3, 1999, pp. 569–573.
doi:10.1109/9.751352
- [25] Sun, W., Khargonekar, P. P., and Shim, P., "Solution to the Positive Real Control Problem for Linear Time-Invariant Systems," *IEEE Transactions on Automatic Control*, Vol. 39, No. 10, 1994, pp. 2034–2046.
doi:10.1109/9.328822
- [26] Safonov, M. G., Jonckheere, E. A., Verma, M., and Limebeer, D. J. N., "Synthesis of Positive Real Multivariable Feedback Systems," *International Journal of Control*, Vol. 45, No. 3, 1987, pp. 817–842.
doi:10.1080/00207178708933772
- [27] Farrell, B. F., "Optimal Excitation of Perturbations in Viscous Shear Flows," *Physics of Fluids*, Vol. 31, No. 8, 1988, pp. 2093–2102.
doi:10.1063/1.866609